Probing the heme-pocket structure of the paramagnetic forms of cytoglobin and a distal histidine mutant using electron paramagnetic resonance

Anda Iulia Ioanitescu, Sabine van Doorslaer, Sylvia Dewilde, Burkhard Endeward, Luc Moens

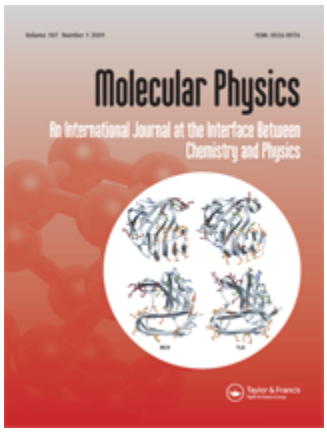

Probing the heme-pocket structure of the paramagnetic forms of cytoglobin and a distal histidine mutant using electron paramagnetic resonance

Journal:	*Molecular Physics*
Manuscript ID:	TMPH-2007-0144.R1
Manuscript Type:	Full Paper
Date Submitted by the Author:	20-Jul-2007
Complete List of Authors:	Ioanitescu, Anda; University of Antwerp, Physics Van Doorslaer, Sabine; University of Antwerp, Physics Dewilde, Sylvia; University of Antwerp, Biomedical Sciences Endeward, Burkhard; JW Goethe University, Physical and Theoretical Chemistry Moens, Luc; University of Antwerp, Biomedical Sciences
Keywords:	globins, electron paramagnetic resonance, heme proteins

Probing the heme-pocket structure of the paramagnetic forms of cytoglobin and a distal histidine mutant using electron paramagnetic resonance

A. Iulia Ioanitescu[1], Sabine Van Doorslaer[1], Sylvia Dewilde[2], Burkhard Endeward[3], Luc Moens[2]

Departments of Physics[1] and Biomedical Sciences[2], University of Antwerp, Antwerp, Belgium,

Institute for Physical and Theoretical Chemistry, JW Goethe University, Frankfurt am Main, Germany[3]

Corresponding author: Prof. Dr. Van Doorslaer, S

Department of Physics

University of Antwerp

Universiteitsplein 1

B-2610 Antwerp, Belgium

Tel: 0032-3-8202461

Fax: 0032-3-8202470

e-mail: Sabine.VanDoorslaer@ua.ac.be

RUNNING TITLE

Heme pocket structure of cytoglobin

ABSTRACT

Cytoglobin is a vertebrate globin with an as yet unidentified function. In this work, S- and X-band pulsed EPR methods are used to elucidate the heme environment of ferric wild-type human cytoglobin (wt CYGB). The data resolve an earlier conflict between two x-ray diffraction studies, and show that the heme iron is bis-histidine ligated with both Fe-His bonds having comparable strength. Similar X-band EPR techniques are applied to study the heme-pocket environment of the ferric HE7Q mutant of CYGB (HE7Q CYGB). No distal water is found to coordinate to the heme iron contrasting the known metaquo form of the HE7Q mutant of myoglobin. The hyperfine and nuclear-quadrupole couplings of the directly coordinating heme and hisitidine nitrogens in ferric wt CYGB and HE7Q CYGB are derived and compared with known data on other ferric porphyrin compounds and heme proteins. In a final part, X-band CW EPR techniques is used in combination with absorption spectroscopy to investigate the ligation and oxidation state of wt CYGB in *E. coli* cells over-expressing this globin. Wt CYGB is found predominantly in the F8His-Fe^{2+}-E7His form, whereby a small fraction of the protein exhibits the F8His-Fe^{2+}-NO form. All present results will be compared in detail with recent studies on neuroglobin, another member of the vertebrate globin family characterized by a bis-histidine coordination of the heme iron in both its ferrous and ferric form.

1. INTRODUCTION

Cytoglobin (Cygb) is a vertebrate globin present in almost all tissue types [1-3]. The function of cytoglobin is still debated, whereby functions such as an involvement in collagen synthesis, in enzymatic reactions, in the O_2 metabolism and in ROS (reactive oxygen species) signalling pathways have been suggested, for details see reviews [4-6]. The size of the by now identified Cygbs (174-190 amino acids) exceeds that of classical vertebrate myoglobins (Mbs), hemoglobins (Hbs), and neuroglobins (Ngbs), which typically comprise 140-160 residues. The classical globin fold can still be recognized in the Cygb core region, however, unusually long N- and C-terminal regions are found for these proteins [1-9]. The key residues PheCD1, HisE7 and HisF8, which are important for the structure and function in respiratory globins, are conserved in Cygb. The protein is found to be dimeric [8].

The wild-type (wt) Cygb proteins and related mutants have been previously studied by means of different biophysical techniques [8-16]. Although all studies show that the heme iron in wt Cygb is predominantly bis-histidine coordinated both in the deoxy ferrous and in the ferric form, there is an inconsistency in the X-ray data concerning the percentage of penta-coordination versus hexa-coordination and concerning the detailed structure of the heme pocket of ferric human cytoglobin (CYGB) [8-10].

De Sanctis *et al*. [8] have shown that heme hexa-coordination is evident in only one of the two cytoglobin chains of the dimer, whereas an alternate distal conformation with partial heme penta-coordination is found in the other. The Fe-N_ε coordination bond is found to be up to 0.025 nm longer for the distal histidine (E7His) than for the proximal histidine

(F8His) and the histidine planes show a staggering (angle of 60°-80° between the two histidine planes). This structure will be further on referred to as 'model I'. In contrast, Sugimoto *et al*. revealed overall bis-histidine coordination, with only small differences between the two Fe-N_ε coordination bond lengths (d(Fe-N_ε(E7His) = 0.22 nm, d(Fe-N_ε(F8His) = 0.23 nm) [10]. The corresponding angle between the histidine planes is ~60°. This conformation will be referred to as 'model II'. A recent ^{1}H NMR study argued in favour of the second model [16].

Continuous-wave (CW) and pulsed electron paramagnetic resonance (EPR) techniques have been shown to be very valuable tools in the study of paramagnetic metallo proteins [17,18]. We recently demonstrated a strategy of combining pulsed and CW EPR techniques to obtain structural and electronic information concerning the heme-pocket environment of ferric low-spin heme proteins, and applied the method successfully to different globins [19-21]. In the first part of the present work, we will use this approach to solve the outlined ambiguities about the heme-pocket structure of ferric CYGB. We will show that an extension of the methodology to pulsed EPR at S-band frequency is in this case necessary. The EPR parameters will be compared with the NMR data on ferric wt CYGB [16] and also with our earlier EPR results on the ferric forms of tomato hemoglobin and mouse neuroglobin (mNgb), both proteins showing bis-hisitidine coordination [20,21].

In the second part, pulsed EPR methods are used to monitor the effect of a point mutation at the E7 position (E7H->E7Q) of CYGB. The EPR data of ferric HE7Q CYGB will be compared with our earlier study on the E7Q mutant of human neuroglobin (NGB) [22].

In the last part, we use CW EPR in combination with absorption spectroscopy to determine whether ferrous wt CYGB is capable of capturing the NO generated by the anaerobically grown *E. coli* cells in which the protein is over-expressed. A similar approach led to important information on the potential involvement of ferrous neuroglobin in the NO metabolism [23,24].

2. MATERIALS AND METHODS

2.1. Materials

E. coli cell cultures for NO-binding experiments. The expression plasmid (CYGB cDNA) was transformed in the *E. coli* strain BL21(DE3)pLysS. The cells were grown at 298 K in TB medium (1.2% bactotryptone, 2.4% yeast extract, 0.4% glycerol, 72 mM potassium phosphate buffer, pH7.5) containing 200 μg ml^{-1} ampicillin, 30 μg ml^{-1} chloramphinicol and 2.5 mM δ-aminolevulinic acid until OD=0.8. The culture was then induced by the addition of isopropyl-1-thio-D-galactopyranoside to a final concentration of 0.4 mM, and expression was continued over night. The cells were harvest and resuspended in lysis buffer (50mM Tris-HCl, pH 8.0, 1mM EDTA, 0.6 mM dithiotreitol). Note that this procedure leads to a small amount of the (heme-containing) holo-protein being formed in the cytosol of the *E. coli* bacteria, whereby the majority of the protein is found in its (heme-free) apo-form in inclusion bodies.

Expression and purification of the CYGB protein. *E. coli* cells were grown in TB medium, as explained above, except that δ-aminolevulinic acid was omitted. Overexpression of CYGB led to production of inclusion bodies. Cells were harvested and resuspended in 50 mM Tris-HCl, pH 7.5, 0.5 M NaCl, 1 mM EDTA, 1 mM PMSF and 5 mM dithiothreitol. The apo-form of CYGB was purified as previously described [25]. The heme-containing holo-CYGB was prepared by titration of the expressed apo-CYGB with equimolar amounts of hemin. Replacement of the distal His (E7) by Gln was performed on CYGB using QuickChange™ site-directed mutagenesis method (Stratagene). The HE7Q mutant was over-expressed, isolated and purified by the same method as CYGB.

For the absorption experiments on the purified proteins, protein concentrations of typically ~60 μM in Tris buffer (pH 8.5) were used. The absorption experiments on the *E. coli* cell cultures were performed on diluted cell suspensions.

For the EPR measurements, 40 % of glycerol was added to all samples as a cryoprotectant. The protein (heme) concentration was taken between 1 and 4 mM.

The deuterium-exchange experiments were done in the following way. The protein was first lyophilised, and afterwards resuspended in deuterated buffer at pH 8.5 (buffer made using D_2O (99.999 atom % D), deuterium chloride (35 wt % in D_2O, 99 atom % D), deuterated Tris buffer (99 atom % D) and deuterated d_8-glycerol (98 atom % D) (all from Sigma-Aldrich)). The protein solution was then kept for 10 hours at 4°C to allow for substantial deuterium exchange.

2.2. Spectroscopy

UV/Vis Optical measurements were performed on a CARY-5 UV-Vis-NIR spectrophotometer (Varian, Palo Alto, California). All optical spectra were measured in the range from 350 to 700 nm.

Continuous-wave Electron Paramagnetic Resonance (CW EPR). CW-EPR spectra were recorded with a Bruker ESP300E spectrometer (microwave (mw) frequency 9.43 GHz) equipped with a gas-flow cryogenic system, enabling operation from room temperature down to 2.5K. All spectra were recorded with 10 mW mw power, a field modulation of 0.5 mT at 100 kHz. The magnetic field calibration was done using an NMR Gaussmeter (Bruker ER 035 M). All EPR spectra were simulated with EasySpin [26].

Pulsed Electron Paramagnetic Resonance Experiments. X-band pulsed EPR experiments were carried out on a Bruker ESP 380E spectrometer (mw frequency 9.76 GHz) equipped with a liquid-helium cryostat from Oxford Inc. The S-band EPR experiments were performed on a home-built pulsed S-band EPR spectrometer [27], mw frequency 3.4 GHz). The spectrometer is controlled with Xepr via an ELEXSYS console including SpecJet and PatternJet (Bruker BioSpin, Rheinstetten, Germany.) The probe is an ER 4118CF liquid helium flow cryostat with a Flexline (Bruker BioSpin, Rheinstetten, Germany) cavity holder and a home build bridged-loop-gap resonator. All experiments were performed at a temperature of 6 K with a repetition rate of 1 kHz.

X-band three-pulse ESEEM (electron spin echo envelope modulation) experiments [17] The pulse sequence used was $\pi/2$-τ-$\pi/2$-T-$\pi/2$-τ-*echo* with pulse lengths $t_{\pi/2}$=16 ns. The time interval T was varied from 96 ns to 4192 ns in steps of 16 ns, whereas the time interval τ was varied from 96 ns to 416 ns in steps of 16 ns. A four-step phase cycle was used to eliminate the unwanted echoes.

HYSCORE (hyperfine sublevel correlation) spectroscopy experiments [28] were carried out with the pulse-sequence $\pi/2$-τ-$\pi/2$-t_1-π-t_2-$\pi/2$-τ-*echo*. An eight-step phase cycle was performed to eliminate unwanted echo contributions. The following parameters were used: pulse lengths of $t_{\pi/2}$=16 ns and t_{π}=16 ns for X-band and $t_{\pi/2}$=24 ns and t_{π}=44 ns for S-band, starting times of 96 ns for t_1 and t_2 and time increments of 16 ns (data matrix 300 x 300). Different τ values were taken to reduce the blind spots. In some cases, the second and third $\pi/2$ pulse were replaced by matching pulses [29].

Data manipulation

The individual time traces of all ESEEM spectra were baseline corrected with a third-order polynomial, apodized with a Hamming window and zero-filled. For the three-pulse ESEEM and combination-peak (CP) spectra, the absolute value spectrum was calculated after 1D Fourier transformation. In order to get a blind-spot free 1D-CP spectrum the τ traces were summed after 1D Fourier transformation. The proton combination frequencies in the 1D-CP spectra were analysed using the procedure outlined in references [19] and [30]. For the HYSCORE spectra, the absolute value spectra were calculated after 2D Fourier transformation. The HYSCORE spectra were simulated using a program developed at the ETH Zurich ([31], time-domain simulation) and EasySpin ([26], frequency-domain simulation).

3. RESULTS

3.1. The heme-pocket structure of ferric wt CYGB

Figure 1a depicts the CW-EPR spectrum of a frozen solution of ferric wt CYGB. Apart from the broad feature in the 400-600 mT region, that could be identified as a base-line drift, the spectrum consists of the typical features of high-spin (HS) and low-spin (LS) ferric species. The g values of the LS component were already determined before [15] (g_x=1.20 (±0.08), g_y=2.08(±0.02), g_z=3.20 (±0.02)) and agree with a bis-histidine coordinated heme. The LS spectrum is only visible at temperatures lower than 40 K, which agrees with what is typically found for so-called highly-anisotropic LS (HALS) ferric heme complexes (maximal g value ≥ 3.20) [32]. The fact that an HS form is identified in the CW-EPR spectrum may corroborate model I [8]. Indeed, ferric heme complexes are found to be in an HS state when no ligand or a weak ligand, such as H_2O, is coordinating from the distal side and the CW-EPR spectrum thus seems to support a mixed state of the protein. However, the appearance of the HS signal was found to strongly depend on the protein batch. For some batches, the HS feature was almost non-existing. This indicates that the presence of the HS form is linked to the protein manipulations and that only the bis-histidine coordinated LS form is relevant. Because of the fact that CYGB is expressed in inclusion bodies and the refolding of the native protein has to be done *in vitro*, the efficiency of the refolding may vary in different batches, which might be the reason for the observed batch-dependent differences in the HS fractions. The observation of only one LS form argues against the existence of different heme coordinations as proposed in model I. Finally, the EPR spectra of the full length ferric wt CYGB were found to be identical to

those of wt CYGB missing the C- and N-termini (data not shown), indicating that the unusual C- and N-terminal sequences do not influence the heme-pocket structure.

In our previous work, we outlined a pulsed EPR strategy that allows determination of the position of the histidine planes in the heme pocket of bis-hisitidine-coordinated low-spin ferric heme proteins [19-21]. This strategy involves three steps: (1) the determination of the orientation of the principal ***g*** axes in the molecular frame via the analysis of the principal hyperfine and nuclear-quadrupole axes of the heme nitrogens in the ***g*** tensor frame, (2) the analysis of the hyperfine tensors of the nearest histidine protons in the ***g*** tensor frame to gain information on the positioning of the His ligands in the heme pocket, and (3) a control experiment in which the orientation of the hyperfine and nuclear-quadrupole axes of the iron-coordinating hisitidine nitrogens versus the principal ***g*** axes is determined. In order to obtain this information, X-band nitrogen HYSCORE experiments (steps 1 and 3) and X-band proton HYSCORE and combination-peak (CP) experiments (step 2) need to be performed.

Figure 2a and b show the X-band nitrogen HYSCORE spectra taken at an observer position corresponding to $g=g_z$ and $g=g_y$. Additional X-band HYSCORE spectra were taken for various magnetic-field settings between these two observer positions (see supplementary material). Ferric wt CYGB is characterized by a larger ***g*** anisotropy than any of the other systems we studied before [19-21]. Because of this ***g*** anisotropy and large g strain effects, the electron-spin-echo intensity at observer positions near $g=g_x$ is very low and no X-band HYSCORE spectra could be recorded within realistic measurement times. After long accumulation times, an X-band three-pulse ESEEM spectrum could be obtained at this position (Figure 3a). This spectrum reveals only signals stemming from the nearby

nitrogens and not from the nearby protons (ν_H = 23.1 MHz, a value too high to be observed with ESEEM). In fact, in the X-band HYSCORE and CP experiments, the proton frequencies could only be observed for magnetic-field settings corresponding to g values near g_z (Figure 4a). In an earlier work, Astashkin *et al*. already showed that pulsed EPR experiments performed at lower mw frequencies can help in the elucidation of the heme environment of LS ferric heme proteins [30] (*cf*. field dependence of g strain and nuclear Zeeman effect). We therefore performed HYSCORE experiments at S-band mw frequencies. In the system under study, the echo intensity was, unfortunately, still found to be very small for magnetic field positions corresponding to $g \approx g_x$, and only poor quality HYSCORE spectra could be recorded (Figure 3b). Although the S-band proton HYSCORE spectra allowed for a better characterization of the proton hyperfine values at the observer positions near $g=g_y$ (Figure 4b), little information could be obtained about the proton couplings at the high-field positions (Figure 3b). This clearly puts a limitation to the amount of structural information that can be obtained from the proton hyperfine analysis.

The X-band HYSCORE spectra in Figure 2a and 2b look quite similar to the ones observed earlier for ferric wt mNgb [21] and for ferric tomato hemoglobin [20]. The assignment of the cross peaks is based on earlier work [19-21,33]. In a first step, the hyperfine and nuclear-quadrupole tensors of the heme nitrogens were determined through simulation of the HYSCORE and three-pulse ESEEM spectra. Since both the single-quantum (SQ) and double-quantum (DQ) nuclear frequencies of the heme nitrogens are clearly identifiable in the different spectra, the corresponding spin-Hamiltonian parameters can be determined with quite high accuracy (supplementary material). The principal axes of the hyperfine and nuclear-quadrupole tensors are found to coincide with the ***g*** tensor axes

(Table 1, Figure 5). As outlined in our earlier work, this allows the determination of the position of the principal $\boldsymbol{g}$ tensor frame in the molecular frame, since the largest nuclear quadrupole value lies in the heme plane perpendicular to the Fe-N_{heme} bond [19]. For ferric wt CYGB, the in-plane $\boldsymbol{g_x}$ and $\boldsymbol{g_y}$ axes are found to eclipse the Fe-N_{heme} bonds (Figure 5). This can only be the case when the two Fe-His bonds have a comparable strength [34,35]. Indeed, if the F8His ligand would be stronger bonded to the heme iron than the E7His residue, than the position of the in-plane $\boldsymbol{g_x}$ axis would follow the projection of the F8His plane on the heme plane (i.e. the principal $\boldsymbol{g_x}$ axis would be rotated 20-30^o away from the Fe-N_{heme} bond). In the case both histidines bind equally well to the heme iron, the $\boldsymbol{g_x}$ axis is expected to lie along the mean of the two imidazole-plane orientations (in this case near the Fe-N_{heme} axis). The orientation of the $\boldsymbol{g}$-tensor axes thus agrees with model II and clearly disagrees with model I. Figure 5 shows the orientation of the $\boldsymbol{g}$ tensor axes and the histidine planes in the molecular axes based on the combination of model II with the current EPR data.

This assignment is also corroborated by the fact that only one set of cross peaks between the double quantum (DQ) nuclear frequencies is found for the coordinating N_ε of the two axially binding histidines (Figures 2a-b, 3a-b). In the case of a significant difference between the two Fe-N_ε bond lengths, clear differences in the nuclear frequencies would be expected, which were not observed.

The hyperfine and nuclear-quadrupole tensors of the coordinating histidine nitrogens can in principle also be used to obtain information on the relative orientation of the His planes. However, in practice, the orientation of these tensors in the molecular frame cannot be determined accurately, since the SQ cross peaks of the histidine nitrogens are

often masked by the cross peaks stemming from the heme nitrogens [19-21]. Therefore, the spin-Hamiltonian parameters of the histidine nitrogens are only used for control purposes. Since we determined already the validity of model II, we can use the corresponding x-ray data and determine the principal hyperfine (and nuclear-quadrupole) values within the limits posed by the crystallographic orientations.

The optimal principal hyperfine and nuclear-quadrupole values of the histidine-nitrogens are given in Table 1. Figure 5 shows the orientation of the different tensors. In order to obtain high-accuracy simulations of the ESEEM spectra, a seven-spin system should in principle be taken into account (S=1/2 and six nitrogen (I=1)). This is not realistic in terms of computation time. Therefore, all the HYSCORE and three-pulse ESEEM simulations are presented as sums of the HYSCORE spectra of the individual two-spin systems (S=1/2, I=1). This approach will however not reproduce any of the possible combination frequencies. It will also influence the relative peak intensities as is shown in the supplementary materials. Figures 2c,d show the simulations of the X-band HYSCORE spectra obtained at $g=g_z$ and $g=g_y$. Figures 3c,d show the simulations of the X-band three-pulse and S-band HYSCORE spectra at magnetic field setting near g_x. The simulations of the HYSCORE spectra at all recorded magnetic-field settings are overlain with the experimental spectra in the supplementary material.

The X-band proton HYSCORE spectrum at $g=g_z$ shows two distinct proton ridges (Figure 4a). One has a width of about 1.6 MHz and is centred around the (ν_H,ν_H) point. The second ridge (maximal width ~3.9 MHz) is shifted from the (ν_H,ν_H) point along the diagonal (displacement Δ in Figure 4a). This displacement of the proton ridge along the diagonal is directly linked to the anisotropy of the hyperfine tensor [17,36]. In the case of

proton hyperfine couplings, the hyperfine anisotropy is due to the dipolar interaction, which in turn depends on $1/R^3$, with R the distance between the proton and the unpaired electron in a point-dipolar approximation. The largest ridge thus originates from the nearest protons (*i.e*. the nearest histidine protons, $R \approx 0.31$ nm). The smaller ridge is due to protons at larger distances, of which the heme meso protons ($R \approx 0.44$ nm) and the NH proton of the histidine ($R \approx 0.51$ nm) are the nearest to the iron centre. It is clear that only one ridge stemming from the nearest histidine protons is observed. Different ridges would be expected if the Fe-His distance (and thus also the Fe-H distance) would be different for the two axial histidines or if the histidine planes would be strongly tilted. The present finding thus confirms again model II.

As mentioned earlier, the quality of the X- and S-band proton HYSCORE spectra at the other observer positions is quite poor (Figures 3b, 4b) and not sufficient for an accurate determination of the Fe-H distances based on the pulsed EPR data only. Reasonable simulations were obtained when the hyperfine couplings for the nearest histidine protons are taken to be [-2.7 –4.8 6.8] MHz and Euler angles [-45 47 ±30]^{o} (Figures 4c,d). The anisotropy of this tensor agrees with a distance R=0.31 ± 0.02 nm. Furthermore, contributions of the meso-protons and histidine N-H protons are taken into account in these simulations (hyperfine values approximated using the point dipolar approximation and assuming that the isotropic hyperfine coupling is zero). Finally, the many far away protons are mimicked by a proton contribution with hyperfine [-0.1 –0.1 0.2] MHz. The overall agreement with the experimental spectra is satisfactory. However, we should stress again that these simulations are based on the Fe-H distances given by the x-ray data.

3.2. The heme-pocket structure of the ferric form of the HE7Q mutant of CYGB

Figure 1b shows the CW-EPR spectrum of a frozen solution of ferric HE7Q CYGB. The mutation of the E7His to E7Gln will prevent hexa-coordination of the heme iron. The EPR spectrum is indeed dominated by the characteristic contribution of a HS ferric globin. The EPR spectrum essentially arises from the transitions in the lower Kramer doublet and can be described as an effective S=1/2 system, with $g_{\perp}$= 5.85 and $g_{\|}$ = 1.992, because the mw frequency at X-band is much smaller than the zero-field splitting (typically 5-10 cm^{-1}). The X-band CW-EPR spectrum is similar for most HS ferric heme proteins and reveals little information on the presence or absence of a distal water ligand. X-band HYSCORE experiments at the observer position corresponding with g=$g_{\|}$ in combination with deuterium exchange can identify the distal ligation. Figure 6a and 6b show the proton HYSCORE spectra of ferric HE7Q CYGB in a normal and deuterated buffer, respectively. Figure 6c and 6d depict the corresponding HYSCORE spectra in the low-frequency region. We showed recently [22] that the proton HYSCORE of aquometmyoglobin taken at the same observer position exhibits clear cross peaks at (17.9 MHz, 12 MHz), which disappear upon dissolution of aquometmyoglobin in a deuterated buffer. Instead, dominant ^{2}H cross peaks were observed in the (++) quadrant at (2.7 MHz, 1.8 MHz). The proton and deuterium cross peaks could be assigned to the protons/deuterons of distal water in aquometmyoglobin. It is clear that a similar behaviour is not observed for ferric HE7Q CYGB, where the proton HYSCORE spectrum does not show the characteristic cross peaks of the water protons (Figure 6a, region where cross peaks are expected is marked by circles). Deuteration does not lead to the characteristic cross peaks at (2.7 MHz, 1.8 MHz) (Figure 6d), but only two cross peaks on the diagonal at 2.13 and 2.46 MHz are visible.

They are centred around the ^{2}H Larmor frequency and originate from remote deuterium nuclei ($A_z \approx 0$ MHz, $P_z \approx 110$ kHz).

Figure 6e shows the (-+) quadrant of the HYSCORE spectrum of ferric HE7Q CYGB at an observer position corresponding with $g=g_{||}$. The cross peaks stem from the heme and histidine nitrogens. The identification of the cross peaks was done in agreement with earlier study on HE7Q NGB [22]. Figure 6f shows the simulated HYSCORE spectra, for which the hyperfine and nuclear-quadrupole parameters from table 2 were used. The hyperfine couplings of both the heme and histidine nitrogens are positive, as was previously observed for other high spin compounds [37].

3.3. NO binding to ferrous wt CYGB

Our earlier studies revealed that the metabolism of fast growing *E. coli* cell cultures shifts from an aerobic to an anaerobic one, whereby NO is produced by the cell [23,24]. We also showed that, when these cells are over-expressing wild-type neuroglobin or its E7 mutants, the globins can bind nitric oxide, whereby the binding occurs more efficiently to the E7-mutants than to wild-type neuroglobin. These experiments are less obvious to perform in the case of CYGB. The CYGB proteins used in the previous two sections were obtained from *in vitro* refolding of the apo-protein isolated from inclusion bodies. Direct folding of the holo-protein in *E. coli* by providing the cell cultures with δ-amino-levulinic acid leads to a small amount of holo-protein, whereby the majority of the protein remains in the apo-form. The low concentration of the properly folded CYGB in the *E. coli* cells puts a limit to the EPR resolution and thus to the information that can be obtained from the experiments.

Figure 7A shows the optical spectra of *E. coli* cell cultures over-expressing the holo-form of CYGB. The features are typical for ferrous deoxy CYGB (Soret band at 424 nm, α and β bands at 559 and 531 nm, respectively [11,14]), revealing that the majority of the CYGB proteins are in the bis-histidine coordinated LS ferrous state. The corresponding EPR spectrum taken at 10 K (Figure 7B) shows a weak signal typical of a His-Fe^{2+}-NO form of heme proteins [24,38]. Combination of the two experiments thus shows that wt CYGB is predominantly found in its deoxy ferrous hexa-coordinated form, with only a small fraction present in the nitrosyl-ligated ferrous form, as was also observed in the case of wt NGB [23,24].

Figure 7B also shows the CW-EPR spectra of the cell cultures at selected temperatures (the full range from 10 up to 175 K was measured). Although the resolution is low, it is clear that the spectra of wt CYGB-NO are varying with temperature. Two major features are observed in the spectra, respectively characterised by a rhombic and axial ***g*** tensor. The contributions of both species are overlapping. Nevertheless, individual features originating from only one of the species can be recognised in the EPR spectra (arrows in Figure 7B). From this, it becomes clear that the rhombic species dominates at low temperatures. The two contributions and their temperature behaviour are typical for His-Fe^{2+}-NO complexes [38-40]. The rhombic (R) and axial (A) contributions to the EPR spectrum of the His-Fe^{2+}-NO forms of heme proteins are believed to originate from different orientations of the bound NO. The rhombic component is ascribed to a bent end-on coordination of the nitrosyl in which the Fe-N(NO) bond does not coincide with the normal to the heme plane [38,41]. The origin of the A form is still unclear, whereby structures involving the Fe-N(NO) parallel to the porphyrin normal as well as partially

dissociated hexa-coordinated complexes with a rotating NO have been proposed [42]. Note that signals due to *E. coli*-specific iron-sulphur proteins (#) as well as a radical signal (*) can be identified in the EPR spectra of the *E. coli* cultures (see Figure 7B) [24].

Figure 7B depicts also the simulations of the different EPR spectra, obtained using the EPR parameters for both the R and A forms as given in table 3. Due to the poor resolution of the spectra, the error on the simulation parameters is quite high. Nevertheless, the observed trend parallels what was observed for the NO-ligated forms of different neuroglobins and myoglobins [23,24,40].

For all these globins, a decrease of the R/A ratio as a function of temperature was observed, paralleled with a continuous change in the *g* values of the species. This was ascribed to a continuous change in the conformation upon temperature increase [24,38,39].

4. DISCUSSION

4.1. The heme-pocket structure of ferric wt CYGB

The current EPR results fully support the x-ray data of Sugimoto *et al*. (model II, [10]). Although a contribution of a HS heme complex could be detected in the CW-EPR spectra of ferric wt CYGB (Figure 1a), this form was highly batch dependent. This indicates that the most stable heme-pocket conformation of ferric wt CYGB involves bis-histidine ligation of the heme iron and that a transient protein conformation was crystallized by de Sanctis *et al.* (model I, [8]). Note that the proteins used in this study were purified in the same laboratory as the ones used for the x-ray study of de Sanctis *et al*. [8]. It is important to note that the EPR data also show that the unusually long N- and C-terminal regions found for CYGB are not influencing the heme-pocket structure.

The $\boldsymbol{g}$ tensor of ferric wt CYGB is more anisotropic than that of ferric mNgb ($\boldsymbol{g}$ =[1.29, 2.15, 3.12]) [15]. The present study shows that this difference cannot be attributed to an inequivalence in binding for the two axial histidines in ferric wt CYGB, nor does it result from a tilt of the E7His-imidazole plane away from the heme normal. Small differences in the dihedral angles between the axial ligand planes and/or possible H-bonding to the remote nitrogen of the histidines will thus be the cause of this difference. Deuterium exchange experiments were attempted to identify the hyperfine coupling of the histidine NH proton, but no changes in the spectra could be observed (data not shown). This may be due to the low accessibility of the heme-pocket region to water.

As already remarked by Walker [32], the x-ray structure on metCYGB (model II) predicts a smaller dihedral angle between the two axial histidine imidazole planes ($\Delta\phi \approx 56^{o}$) [8] than found for ferric mNgb ($\Delta\phi \approx 59^{o}$) [43]. From this, one would predict a different trend in the principal g values (lower g anisotropy is expected for wt CYGB). The histidine planes are rotated asymmetrically away from N_{heme}-Fe-N_{His} plane in the case of ferric mNgb ($\Delta\phi_{E7His} \approx 40^{o}$ and $\Delta\phi_{E7His} \approx 20^{o}$) [43], whereby a more symmetric distribution is found for ferric wt CYGB. These findings are supported by the fact that the in-plane principal $\boldsymbol{g}$ axes of ferric mNgb are found to be slightly tilted away from the N_{heme}-Fe-N_{heme} ($10^{o} \pm 10^{o}$) [21], where an eclipsing situation is observed in the current study. The small difference in the orientation of the in-plane $\boldsymbol{g}$ tensor axes can however not explain the change in the g anisotropy (if any, the effect would be again opposite). Walker suggested that the discrepancy between the x-ray and EPR data is due to a formation of different hydrogen-bond arrangements in the quite open heme-pocket structure of mNgb upon freezing of the solution [32], although this remains to be confirmed. It should also be noted

that the observed difference in the dihedral angle is close to the margin given by the experimental error of the x-ray data. The extreme flexibility of the heme-pocket region of neuroglobin has been proven using different techniques [44,45,46], including the observation that the principal *g* values of ferric wt NGB change upon disulfide bridge formation [15] and the fact that the E10Lys can bind to the heme iron in HE7Q NGB at high pH [22]. The heme pocket in wt CYGB is buried deeper in the protein matrix, although the effect of temperature-induced formations of H-bonds to water molecules in the heme region cannot be excluded.

The present finding that the in-plane principal ***g*** axes are eclipsing the N_{heme}-Fe-N_{heme} bonds parallels the NMR observation that the magnetic axes are along these bonds [16]. In the NMR analysis, the in-plane direction of the magnetic axes is determined using the meso-^{1}H hyperfine shifts, whereby the assignment of the ***g*** tensor axes in the EPR study is based on the analysis of the ^{14}N hyperfine and nuclear-quadrupole tensors of the heme nitrogens (Table 1). Both approaches lead to the same conclusion showing that the room-temperature (NMR) and frozen-solution (EPR) data are consistent.

Inspection of Table 1 reveals that the principal hyperfine and nuclear-quadrupole values of the pyrrole nitrogens are only marginally influenced by the type and orientation of the axial ligands. This facilitates the ESEEM simulation procedure to determine the orientation of the principal ***A*** and ***P*** axes in the ***g*** tensor frame for unknown ferric heme proteins. As expected, the corresponding couplings of the N_{ε} of the axial imidazole ligands are more sensitive to the change in axial ligation. However, due to considerable spectral overlap (see section 3.1), the experimental error on these parameters is often in the same order of magnitude as the differences between the individual LS forms, rendering an

analysis of the observed trends at this stage difficult. For this reason, the ***A*** and ***P*** tensors of the histidine nitrogens are best not used to determine the orientation of the histidine ligands relative to the magnetic axes. For many low-spin ferric heme systems, this information can be determined from the analysis of the hyperfine couplings of the protons of the axial ligands as was shown in [21-23,30]. However, the present study indicates that this approach can become unreliable for low-spin ferric heme proteins characterized by a large ***g*** anisotropy and significant *g* strain (so-called HALS species). An earlier CW-ENDOR study of cytochrome c_6 from *Anabaena* PCC 7119 where both HALS and a 'normal' LS heme form are present also failed to reproduce the full set of proton hyperfine couplings for the HALS species [33].

4.2. The heme-pocket structure of the ferric form of the HE7Q mutant of CYGB

Our HYSCORE experiments have clearly shown that no distal water molecule is bound to the heme iron in ferric HE7Q CYGB. The same result was found for the HE7Q mutant of NGB [22], but contrasts the observations for HE7Q metmyoglobin, which (partially) retains a water molecule [47,48].

The x-ray studies showed the presence of a large hydrophobic protein cavity (about 240 $Å^3$), forming a wide pocket with a narrow tunnel located between the globin's G and H helices. In the initial part of the cavity, a cluster of three hydrogen-bonded water molecules was reported [8]. The current EPR studies show that the H_2O molecules are not able to propagate to the heme iron in ferric HE7Q CYGB. Absorption and resonance Raman measurements indicated that the ferric form of the HE7A mutant of CYGB is at pH 8 dominantly in a LS ferric form [11]. Redox titration experiments suggested that either the

Cys at the E9 position or the E12Met are the distal ligands of the heme iron, implying a considerable flexibility of the heme pocket. This is clearly not the case for ferric HE7Q CYGB, where the Gln residue prevents large changes in the heme region. This may indicate that the Gln is (weakly) binding to the heme iron. To our knowledge, an amide group has only once been reported as a sixth heme ligand, namely for a cytochrome c from *Rhodobacter sphaeroides* [49]. For this proteins, a His-Fe-Asn ligation was found by x-ray diffraction, and the corresponding EPR spectrum was typical for a HS Fe(III) form. Although our present results cannot proof a (weak) distal Gln ligation in ferric HE7Q CYGB, they also do not disagree with this hypothesis. Furthermore, the fact that ^{2}H signals due to remote deuterium nuclei are observed in the HYSCORE spectra of HE7Q CYGB in D_2O indicates that water can indeed enter the heme pocket but that direct binding of water is prevented by the E7Gln residue. The origin of the observed deuterium coupling cannot be determined, but likely candidates are the exchangeable protons of the E7Cys, E10Arg or E6Lys residues present in the distal side of the heme pocket.

From the HYSCORE simulations, the *z* component of the hyperfine and nuclear quadrupole parameters were determined for both the heme and histidine nitrogens (Table 2). There is no significant difference between these parameters for different high-spin ferric globin systems with varying distal ligation, indicating that these parameters are only marginally sensitive to the nature of the distal ligand.

4.3. *NO binding to ferrous wt CYGB*

When wt CYGB molecules are expressed in anaerobically grown *E. coli* cells, the heme iron is predominantly bis-histidine coordinated, whereby only a small fraction is in the NO-

ligated form (Figure 7). This finding parallels observations for wt mNgb and NGB [23,24]. In the latter cases, it was found that, when the competition with the distal histidine is prevented through mutation of the E7His to Leu, Val or Gln, the nitrosyl ferrous form is dominating. Although an obvious interpretation of these data seems to be that neither neuroglobins nor cytoglobins can play a significant role in the NO metabolism, one should keep in mind that the *E. coli* cells have also a very efficient NO detoxification system (flavorubredoxin [50]). The present observation only indicates that the NO-binding kinetics of wt CYGB do not match *E. coli*'s own defence mechanism against NO, but does not exclude a role in the NO metabolism in eukaryotic cells. In fact, the observation of the ferrous nitrosyl form of wt CYGB in intact *E. coli* cells, even if it is a minority, shows that NO binding may be one of the roles of CYGB and should be investigated in detail.

It is important to note that, at 10K, the R/A ratio is lower for the NO-ligated form of wt CYGB (R/A=1.78) than for the NO-ligated forms of wt NGB (R/A=2.33 [24]), HE7Q NGB (R/A=4 [24]) and HE7L NGB (R/A=4.55 [24]), this becomes already clearly apparent from visual comparison of the spectra (Figure 7B compared with Figure 2 in ref [24]). ENDOR studies on the A and R isomers of horse heart Mb showed that in the two forms, the NO ligand is stabilized by E7His and E11Val, but that the strength of the interaction is different [41].

The current results thus indicate a stronger stabilization of the axial form by the E7His in wt CYGB-NO than in wt NGB-NO. Previous resonance Raman experiments on the CO-ligated forms of ferrous wt NGB [12] and ferrous wt CYGB [11] showed also differences between the CO conformers. In CO-ligated wt CYGB, three conformations of the Fe-CO unit could be detected. Two of them agree with the closed conformation in

which the CO ligand is interacting strongly with E7His (ν_{Fe-CO}=510/518 cm^{-1}), while the third is an 'open conformation', whereby the CO ligand has little interaction with the surrounding amino acids (ν_{Fe-CO}=492 cm^{-1}) [11]. The CO-ligated form of the wt NGB revealed three configurations for the Fe-CO unit [12]. In addition to one 'open' (ν_{Fe-CO}=494 cm^{-1}) and one 'closed' (ν_{Fe-CO}=521 cm^{-1}) conformation, an 'intermediate' conformer is found (ν_{Fe-CO}=505 cm^{-1}), that has also been observed for the CO-ligated form of ferrous myoglobin [51]. This form is not found in CYGB. Our current EPR results show that slight differences can also be observed for the stabilization of the nitrosyl ligand in the NO-ligated ferrous forms of CYGB and NGB.

Acknowledgements

This work was supported by the Fund for Scientific Research-Flanders (FWO) Grant G.0468.03 (to S.V.D.). S. D. is a postdoctoral fellow of the FWO. We wish to thank Prof. Dr. Thomas Prisner from the JW Goethe University, Frankfurt am Main, for the use of the S-band EPR facility.

References:

[1] J.T.III Trent and M.S. Hargrove. *J. Biol. Chem*. **277**, 19538 (2002).

[2] N. Kawada, D.B. Kristensen, K. Asahina, K. Nakatani, Y. Minamiyama, S. Seki and K. Yoshizato. *J. Biol. Chem*. **276**, 25318 (2001).

[3] T. Burmester, B. Ebner, B. Weich, T. Hankeln. *Mol. Biol. Evol.* **19**, 416 (2002).

[4] A. Pesce, M. Bolgnesi, A. Bocedi, P. Ascenzi, S. Dewilde, L. Moens, T. Hankeln, T. Burmester. *EMBO Rep.* **3**, 1146 (2002).

[5] P. Ascenzi, A. Bocedi, D. de Sanctis, A. Pesce, M. Bolognesi, M.C. Marden, S. Dewilde, L. Moens, T. Hankeln, T. Burmester. *BAMBED* **32**, 305 (2004).

[6] A. Pesce, D. de Sanctis, M. Nardini, S. Dewilde, L. Moens, T. Mankeln, T. Burmester, P. Ascenzi, M. Bolognesi. *IUBMB Life* **56**, 657 (2004).

[7] D. Kugelstadt, M. Haberkamp, T. Hankeln, T. Burmester. *Biochem. Biophys. Res. Commun.* **325**, 719 (2004).

[8] D. de Sanctis, S. Dewilde, A. Pesce, L. Moens, P. Ascenzi, T. Hankeln, T. Burmester, M. Bolognesi. *J. Mol. Biol.* **336**, 917 (2004).

[9] D. de Sanctis, S. Dewilde, A. Pesce, L. Moens, P. Ascenzi, T. Hankeln, T. Burmester, M. Bolognesi. *Biochem. Biophys. Res. Commun.* **316**, 1217 (2004).

[10] H. Sugimoto, M. Makino, H. Sawai, N. Kawada, K. Yoshizato, Y.J. Shiro. *Mol. Biol.* **339**, 873 (2004).

[11] H. Sawai, N. Kawada, K. Yoshizato, H. Nakajima, S. Aono, Y. Shiro. B*iochemistry* **42**, 5133 (2003).

[12] H. Sawai, M. Makino, Y. Mizutani, T. Ohta, H. Sugimoto, T. Uno, N. Kawada, K. Yoshizato, T. Kitagawa, Y. Shiro. *Biochemistry* **44**, 13257 (2005).

[13] D. Hamdane, L. Kiger, S. Dewilde, B.N. Green, A. Pesce, J. Uzan, T. Burmester, T. Hankeln, M. Bolognesi, L. Moens, M.C. Marden. *J. Biol. Chem.* **278**, 51713 (2003).

[14] A. Fago, C. Hundahl, S. Dewilde, K. Gilany, L. Moens, R.E. Weber. *J. Biol. Chem.* **279**, 44417 (2004).

[15] E. Vinck, S. Van Doorslaer, S. Dewilde, L. Moens. *J. Am. Chem. Soc.* **126**, 4516 (2004).

[16] V. Bondarenko, S. Dewilde, L. Moens, G.N. La Mar. *J. Am. Chem. Soc.* **128**, 12988 (2006).

[17] A. Schweiger, G. Jeschke. *Principles of Pulse Electron Paramagnetic resonance*, Oxford University press, Oxford (2001).

[18] T. Prisner, M. Rohrer, F. MacMillan. *Annu. Rev. Phys. Chem.* **52**, 279 (2001).

[19] E. Vinck, S. Van Doorslaer. *Phys. Chem. Chem. Phys.* **6**, 5324 (2004).

[20] A.I. Ioanitescu, S. Dewilde, L. Kiger, M.C. Marden, L. Moens, S. Van Doorslaer. *Biophys. J.* **89**, 2628 (2005).

[21] E. Vinck, S. Van Doorslaer, S. Dewilde, G. Mitrikas, A. Schweiger, L. Moens. *J. Biol. Inorg. Chem.* **11**, 467 (2006).

[22] F. Trandafir, P. Ter Heerdt, M. Fittipaldi, E. Vinck, S. Dewilde, L. Moens, S. Van Doorslaer. *Appl. Magn. Reson.* in press (2007).

[23] S. Van Doorslaer, S. Dewilde, L. Kiger, S. Nistor, E. Goovaerts, M.C. Marden, L. Moens. *J. Biol. Chem.* **278**, 4919 (2003).

[24] F. Trandafir, S. Van Doorslaer, S. Dewilde, L. Moens. *Biochim. Biophys. Acta* **1702**, 153 (2004).

[25] D. de Sanctis, S. Dewilde, A. Pesce, P. Ascenzi, T. Burmester, T. Hankeln, *Acta Crystallog. Sect. D* **59**, 1285 (2003).

[26] S. Stoll, A. Schweiger. *J. Magn. Reson*. **177**, 390 (2005).

[27] Weber, A., Rohrer, M., Törring, J. T., and Prisner, T. F. (1998) A CW and pulsed S-band spectrometer. In: Ziessow, D., Lubitz, W., and Lendzian, F. (eds). *Proceedings of the 29th Congress AMPERE/13th ISMAR*

[28] P. Höfer, A. Grupp, H. Nebenführ, M. Mehring. *Chem. Phys. Lett.* **132**, 279 (1986).

[29] G. Jeschke, R. Rakhmatullin, A. Schweiger. *J. Magn. Reson.* **131**, 261 (1998).

[30] A.V. Astashkin, A.M. Raitsimring, F.A. Walker. *Chem. Phys. Lett*. **306**, 9 (1999).

[31] Z.L. Madi, S. Van Doorslaer, A. Schweiger. *J. Magn. Reson*. **154**, 181 (2002).

[32] F.A. Walker. *J. Biol. Inorg. Chem.* **11**(4), 391 (2006).

[33] I. García-Rubio, J.I. Martínez, R. Picorel, I. Yruela, P.J. Alonso. *J. Am. Chem. Soc*. **125**, 15846 (2003).

[34] N.V. Shokhirev, A. Walker, *JBIC* **3**, 581 (1998).

[35] N. V. Shokhirev, A. Walker. *JACS* **120,** 981 (1998).

[36] A. Pöppl, M. Gutjahr, M. Hartmann, W. Bohlmann, R. Böttcher, *J. Phys. Chem. B* **102**, 7752 (1998).

[37] C.P. Scholes, A. Lapidot, R. Mascarenhas, T. Inubushi, RA. Isaacson, G. Feher. *J. Am. Chem. Soc.* **104**, 2724 (1982).

[38] P.P. Schmidt, R. Kappl, J. Hüttermann. *Appl. Magn. Resn.* **21**, 423 (2001).

[39] E. Wajnberg, M.P. Linhares, L.J. El-Jaick, G. Bemski. *Eur. Biophys. J.* **21**, 57 (1992).

[40] M. Flores, E. Wajnberg, G. Bemski. *Biophys. J.* **73**, 3225 (1997).

[41] M. Flores, E. Wajnberg, G. Bemski. *Biophys. J.* **78**, 217 (2000).

[42] S. Patchkovskii, T. Ziegler. *Inorg. Chem.* **39,** 5354 (2000).

[43] B. Vallone, K. Nienhaus, M. Brunori, G.U. Nienhaus. *Proteins* **56**, 85 (2004).

[44] B. Vallone, K. Nienhaus, A. Matthes, M. Brunori, G.U. Nienhaus. *Proc. Natl. Acad. Sci. USA* **101**, 17351 (2004).

[45] T. Uno, D. Ryu, H. Tsutsumi, Y. Tomisugi, Y. Ishikawa, A.J. Wilkinson, H. Sato, T. Hayashi. *J. Biol. Chem.* **279**, 5886 (2004).

[46] D. Hamdane, L. Kiger, S. Dewilde, B.N. Green, A. Pesce, J. Uzan, T. Burmester, T. Hankeln, M. Bolognesi, L. Moens, M.C. Marden, *J. Biol. Chem.* **278**, 51713 (2003).

[47] M. Ikeda-Saito, H. Hori, L.A. Andersson, R.C. Prince, I.J. Pickering, G.N. George, C.R. Sanders, R.S. Lutz, E.J. McKelvey, R. Mattera. *J. Biol. Chem.* **267**, 22843 (1992).

[48] K. Rajarthnam, G.N. La Mar, M.L. Chiu, S.G. Sligar, J.P. Singh, K.M. Smith. *J. Am. Chem. Soc.* **113**, 7886 (1991).

[49] D. Leys, K. Backers, T.E. Meyer, W.R. Hagen, M.A. Cusanovich, J.J. Van Beeumen. *J Biol Chem*. **275**, 16050 (2000).

[50] A.M. Gardner, R.A. Helmick, P.R. Gardner. *J. Biol. Chem.* **277**, 8172 (2002).

[51] D.L. Rousseau, J.M. Friedmann, *Biological Application of Raman Spectroscopy* (Spiro, T.G., Ed.) vol. 3, pp133-215, John Wiley & Sons, New York (1988).

Tables

Table 1. Comparison of the principal hyperfine and nuclear-quadrupole values of the heme and histidine ^{14}N nuclei of ferric wt CYGB and other bis-imidazole coordinated iron-porphyrin systems. The orientation of the principal hyperfine and nuclear quadrupole tensor axes are given in Figure 5 for the ferric wt CYGB case.

	A_1 /MHz	A_2 /MHz	A_3 /MHz	P_1 /MHz	P_2 /MHz	P_3 /MHz	Ref.
			Pyrrole nitrogens				
Ferric wt CYGB	-4.0 (± 0.2)	-4.1 (± 0.2)	-5.45 (± 0.2)	-0.50 (± 0.05)	0.92 (± 0.05)	-0.42 (± 0.05)	This work
Ferric wt mNgb	-4.8	-4.8	-5.7	-0.52	0.95	-0.43	[21]
Ferric tomato Hb	-4.5	-3.6	-5.4	-0.46	0.88	-0.42	[20]
FeTPP(4-MeIm)$_2$	-4.2	-4.2	-5.7	-0.51	0.93	-0.42	[19]
			Imidazole nitrogens				
Ferric wt CYGB	-5.9 (± 0.4)	-4.7 (± 0.4)	-5.0 (± 0.2)	0.34 (± 0.10)	0.56 (± 0.10)	-0.90 (± 0.05)	This work
Ferric wt mNgb	-5.65 -5.65	-5.25 -5.25	-4.9 -4.9	0.16 0.3	0.64 0.55	-0.8 -0.85	[21]
Ferric tomato Hb	-5.1	-6.4	-4.9	0.04	0.76	-0.8	[20]
FeTPP(4-MeIm)$_2$	-5.7	-6.2	-5.3	0.34	0.51	-0.85	[19]

Table 2. Hyperfine and nuclear-quadrupole parameters for the heme and histidine nitrogens of different ferric high-spin systems.

	A_z (MHz)	P_z (MHz)	Reference
N_{heme}/ HE7Q CYGB [a]	7.15 ±0.2	0.95 ±0.05	This work
N_{heme}/ E7Q-NGB[a]	7.25	0.95	[22]
N_{heme}/ Mb[b]	7.11	1.04	[37]
$N_{\varepsilon\ His}$/ HE7Q CYGB[a]	12.35 ±0.2	-1.20 ±0.05	This work
$N_{\varepsilon\ His}$/ E7Q-NGB[a]	12.0	-1.2	[22]
$N_{\varepsilon\ His}$/ Mb[c]	11.55	-1.12	[37]

[a] Principal axes of **A** and **P** were taken to coincide with the principal **g** tensor axes.

[b] **z** is tilted 7.6° away from the heme normal.

[c] **z** is along the heme normal, y is in the histidine plane, rotated 11° away from the N_{heme}-Fe- N_{heme} axis.

Table 3. The temperature dependence of the principal *g* values for the rhombic and axial component in the EPR spectra of CYGB, obtained from the simulations. The ratio of the rhombic versus axial species is also indicated

T (K)	Rhombic signal			Axial signal		R/A
	g_1 (±0.003)	g_2 (±0.005)	g_3 (±0.01)	$g_\perp$ (±0.005)	$g_\parallel$ (±0.01)	(±5%)
10	2.075	2.012	1.98	2.037	1.99	64/36
40	2.073	2.013	1.98	2.037	1.99	56/44
70	2.072	2.013	1.98	2.037	1.99	50/50
100	2.071	2.013	1.98	2.037	1.99	47/53

For the rhombic species, the hyperfine values of the ^{14}N(NO) ligand were taken to be: A_1=39 ± 5 MHz, A_2=45 ± 10 MHz, A_3=43 ± 5 MHz; the hyperfine values of the proximal ^{14}N of the proximal histidine were taken to be: A_1=15 ± 5 MHz, A_2=14 ± 10 MHz, A_3=30 ± 5 MHz

Figure captions.

Figure 1. Experimental (solid line) and simulated (dashed line) X-band CW-EPR spectra of a frozen solution of ferric wt CYGB (a) and of ferric HE7Q CYGB (b) (both pH 8.5). The spectra are recorded at 10K. HS stands for high spin; the * indicate contributions of non-heme iron and the three arrows in figure (a) indicate the principal g values of the low-spin ferric form.

Figure 2. Experimental and simulated X-band nitrogen HYSCORE of a frozen solution of ferric wt CYGB at pH 8.5. (a) Experimental HYSCORE spectrum at an observer position $g=g_z$. The spectrum is the sum of experiments at τ = 96, 128 and 176 ns. (b) Experimental HYSCORE spectrum at an observer position $g=g_y$. The spectrum is the sum of experiments at τ = 96, 144, 152 and 176 ns. In all spectra, the double-quantum (DQ) frequencies of the iron-coordinating heme and histidine nitrogens are indicated. (c), (d) Simulation of (a), (b), respectively. The simulation parameters are given in Figure 5 and Table 1.

Figure 3. (a) Experimental X-band three-pulse ESEEM at an observer position $g=g_x$. The spectrum is the sum of experiments for τ varying from 96 ns to 416 ns in steps of 16 ns. (b) Experimental S-band HYSCORE spectrum at an observer position corresponding to g=1.38. (c), (d) Simulation of (a), (b), respectively. The simulation parameters are given in Figure5 and Table 1.

Figure 4. Proton HYSCORE spectra of a frozen solution of ferric wt CYGB at pH 8.5. (a) Experimental X-band proton HYSCORE spectrum at an observer position $g=g_z$. The spectrum is the sum of experiments at τ = 96, 128 and 176 ns. (b) Experimental S-band proton HYSCORE spectrum at an observer position $g=g_y$. The spectrum was taken for τ = 372 ns. (c) Simulation of (a) using the proton hyperfine parameters given in the text. (d) Simulation of spectrum (b) using the proton hyperfine parameters given in the text.

Figure 5. The heme-pocket structure of ferric wt CYGB (proximal side up). The orientation of the ***g*** matrix and the nuclear quadrupole tensors of the histidine and pyrrole nitrogens are indicated as determined by linking the results from this study (Table 1) with the X-ray model II. The numbers between the brackets refer to the principal hyperfine and nuclear quadrupole values in MHz along these principal axis. $\Delta\varphi_{E7His}$=24 ($\pm10^o$) and $\Delta\varphi_{F8His}$=22 ($\pm10^o$).

Figure 6. HYSCORE spectra of ferric HE7Q CYGB in varying buffers (pH 8.5) taken at an observer position corresponding to $g=g_{\|}$. (a) Proton HYSCORE spectrum; aqueous buffer. The circles indicate the position where the cross peaks due to distal water protons should appear in case of an aquomet form. τ was taken to be 216 ns. (b) Proton HYSCORE spectrum; deuterated buffer. τ was taken to be 216 ns. (c) HYSCORE spectrum in region [0-5,0-5] MHz; aqueous buffer. The cross peaks due to the remote histidine nitrogen are indicated. τ was taken to be 120 ns. (d) HYSCORE spectrum in region [0-5,0-5] MHz; deuterated buffer. The cross peaks due to ^{2}H are highlighted. τ was taken to be 120 ns. (e) HYSCORE spectrum in region [-13-0,0-13] MHz. τ was taken to be 120 ns. The single-

quantum (SQ) and double-quantum (DQ) cross peaks of the heme and histidine iron-coordinating nitrogens are indicated. (f) Simulation of spectrum (e) using the hyperfine and nuclear-quadrupole values given in Table 2.

Figure 7. (A) Optical spectrum of an *E. coli* cell culture overexpressing wt CYGB. (B) Experimental (solid line) and simulated (dashed line) X-band CW-EPR spectra of *E. coli* cells overexpressing wt CYGB as a function of temperature. # indicates the contribution of an *E. coli* iron-sulfur protein, * indicates the position of an organic radical. A and R indicate distinctive spectral features that stem respectively from the axial and rhombic His-Fe-NO species of NO-ligated ferrous wt CYGB.

FIGURE 1

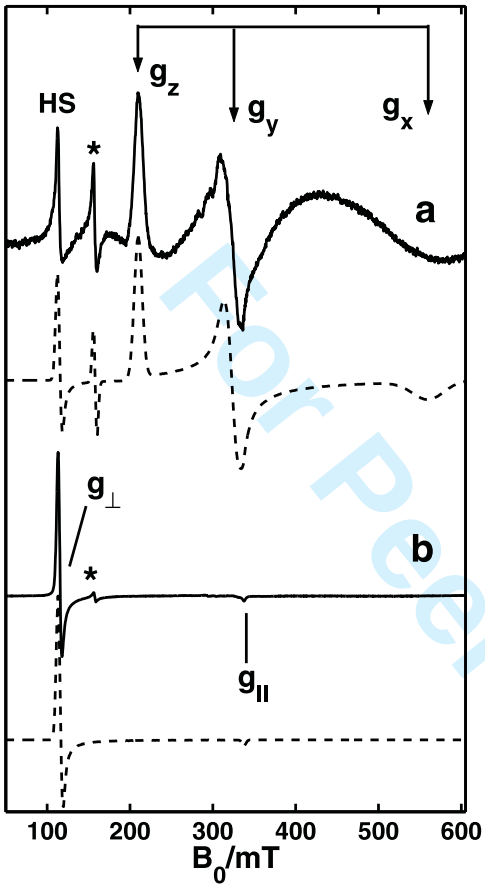

FIGURE 2

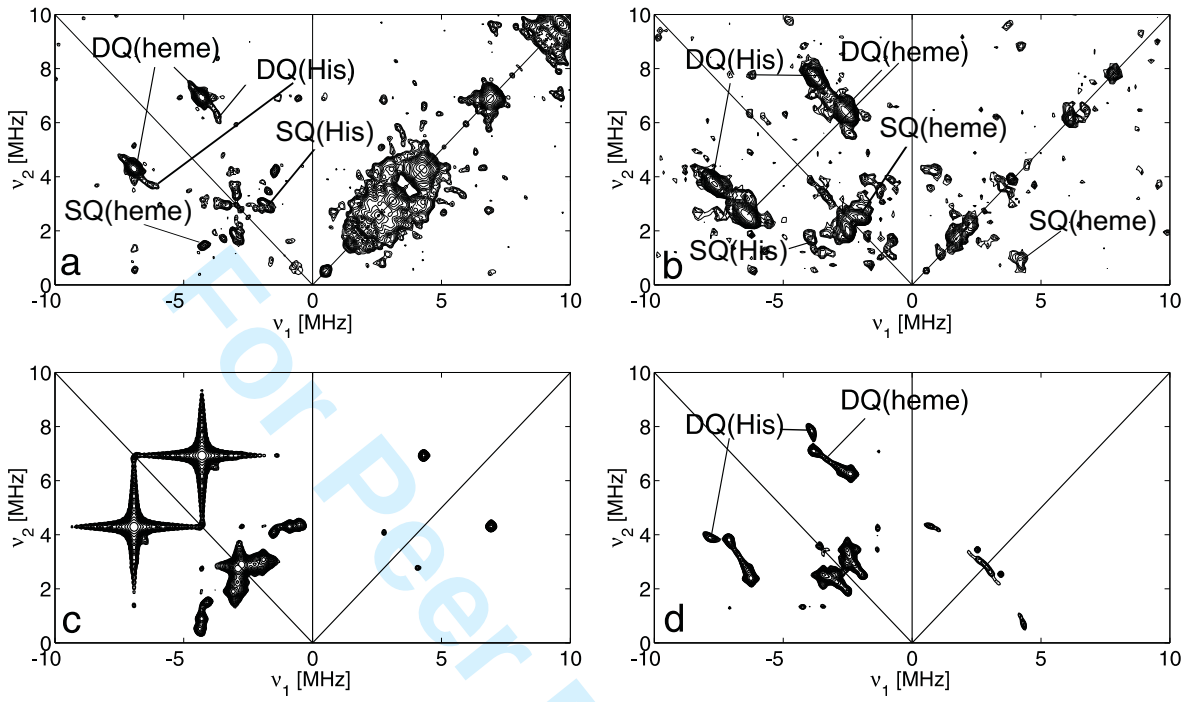

FIGURE 3

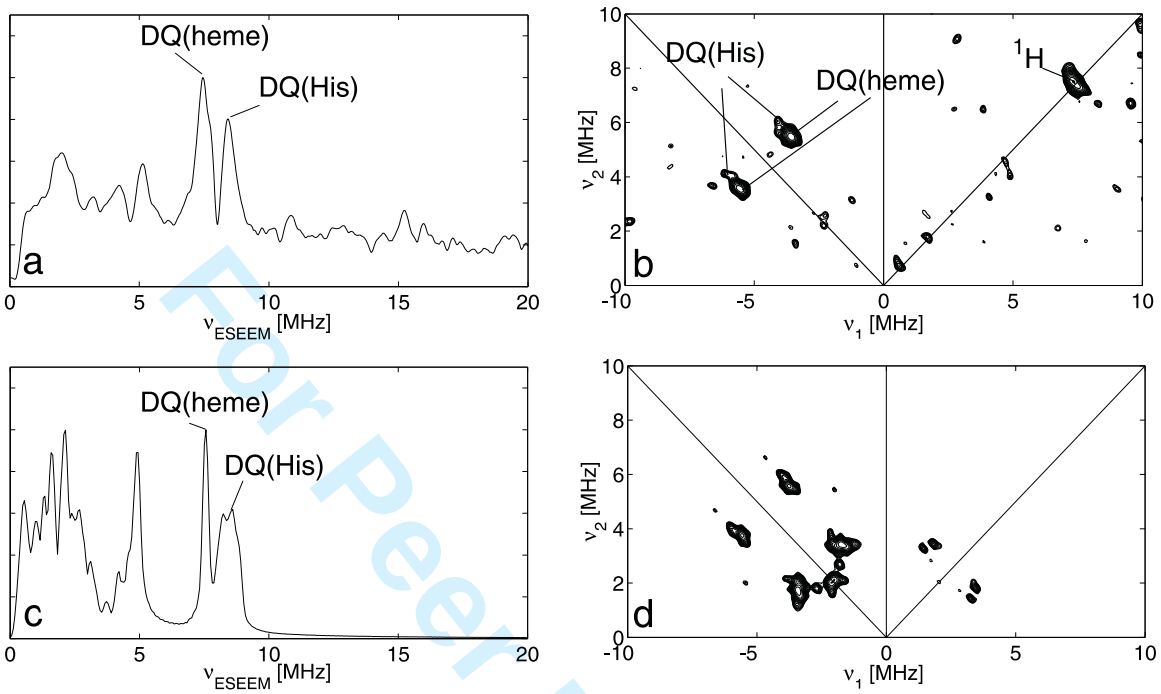

FIGURE 4

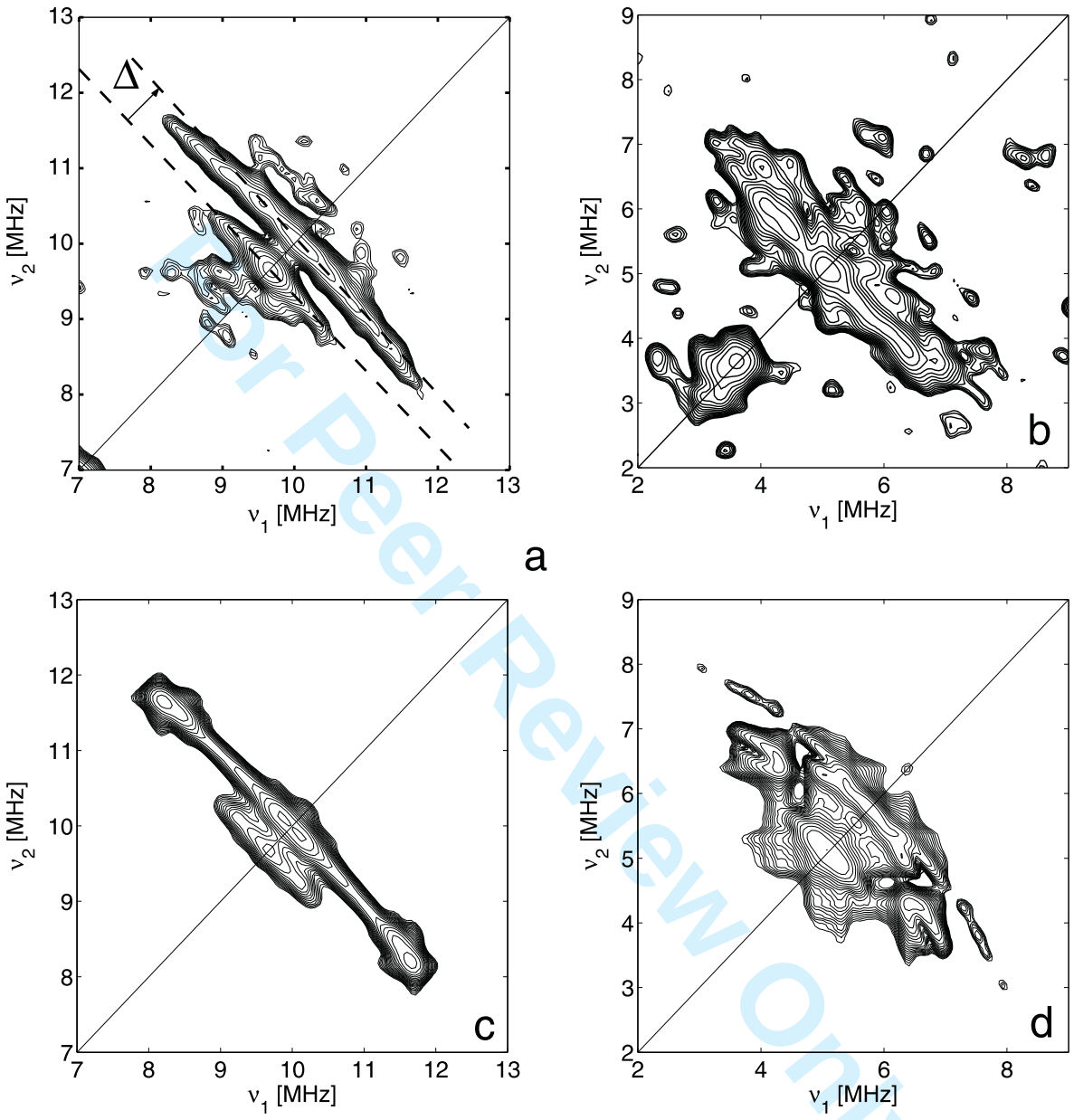

FIGURE 5

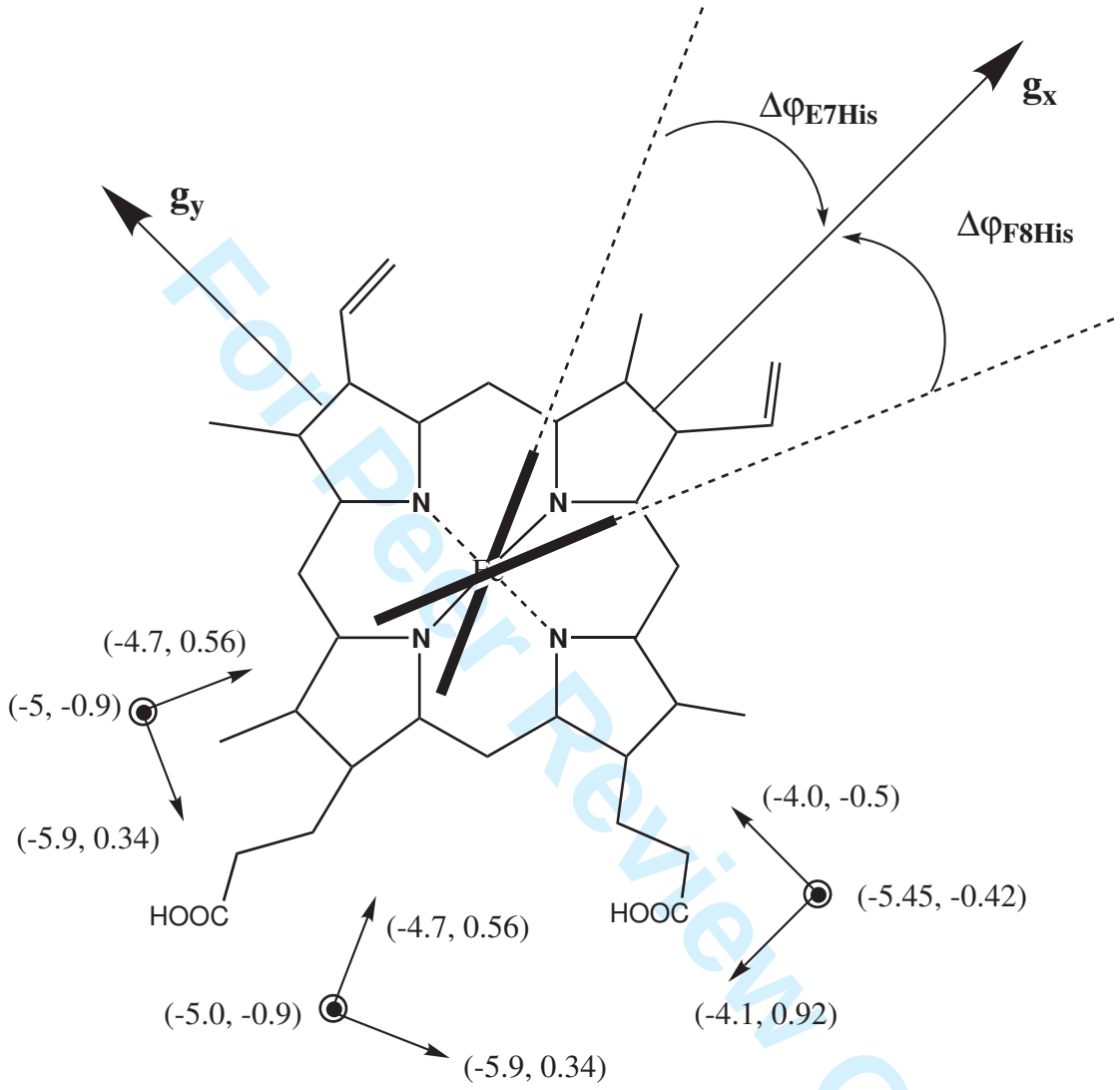

FIGURE 6

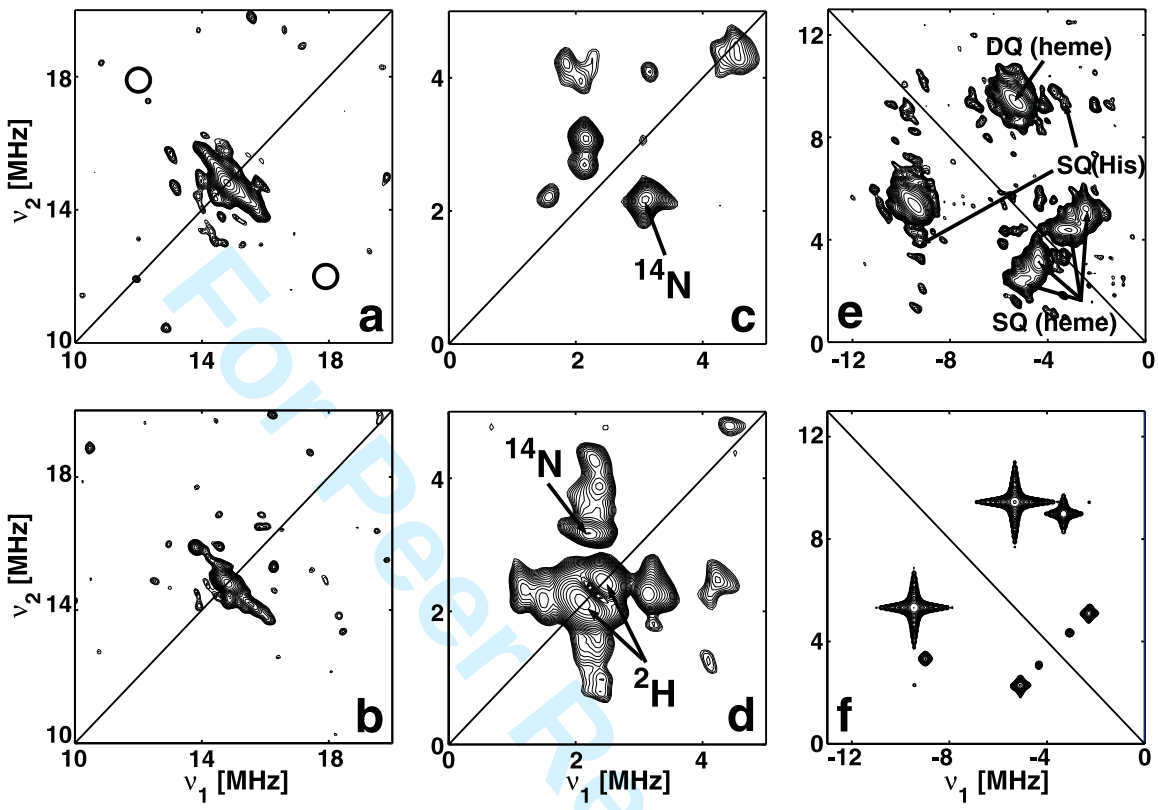

FIGURE 7

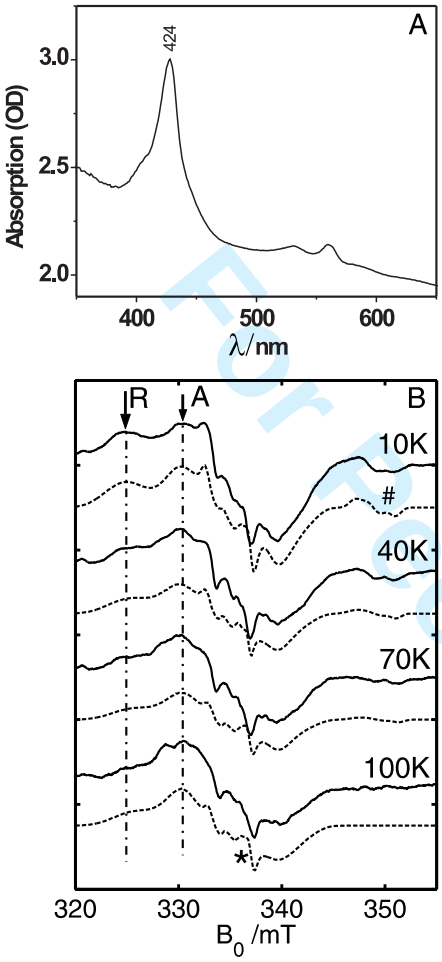

SUPPLEMENTARY MATERIAL to

Probing the heme-pocket structure of the paramagnetic forms of cytoglobin and a distal histidine mutant using electron paramagnetic resonance

A.Iulia Ioanitescu *et al.*

Simulations of the HYSCORE spectra

a) Spectral contributions of heme nitrogens.

Red: simulated spectra; Blue: experiments

The simulated spectra are the sum of the individual contributions of all heme nitrogens (simulation parameters given in Table 1 of the main text).

X-band HYSCORE spectra:

B_0=2268 G (g=g_z)

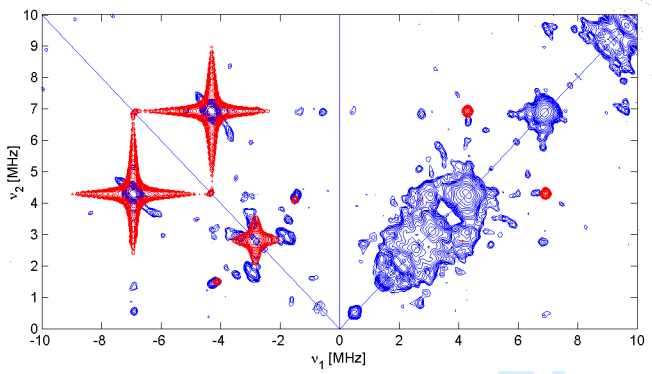

B_0=2500 G

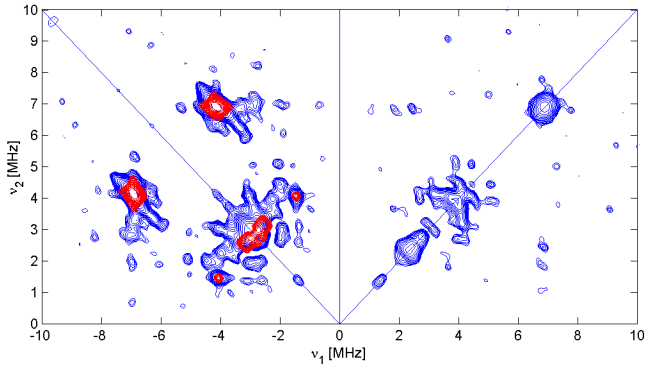

B_0=2900 G

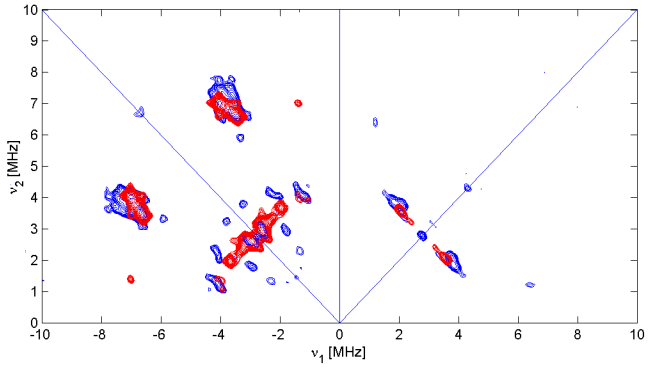

B_0=3123 G

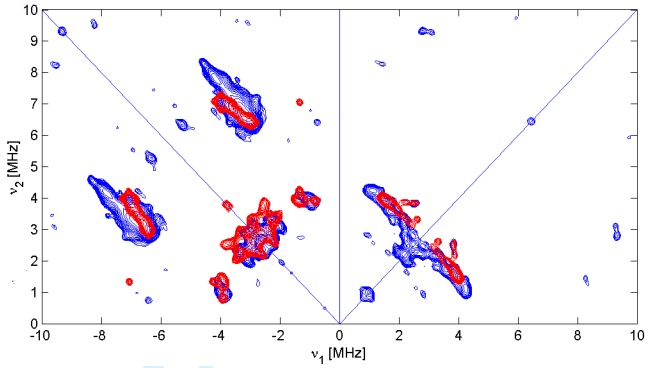

B_0=3374 G (g=g_y)

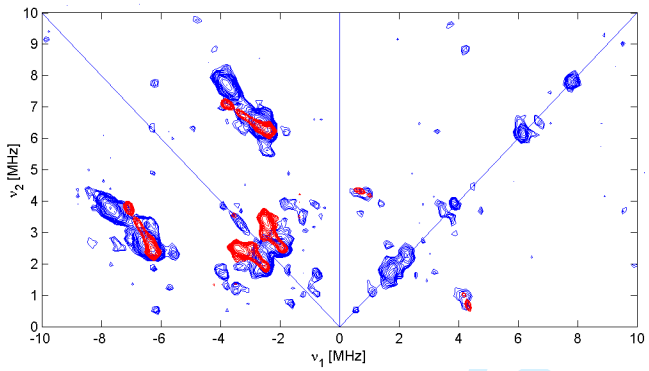

S-band HYSCORE

B_0=1750 G (g≈g_x)

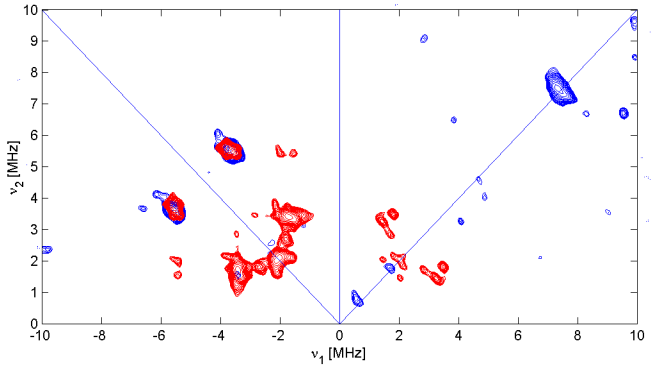

X-band 3-pulse ESEEM

B_0=5432 G (g=g_x)

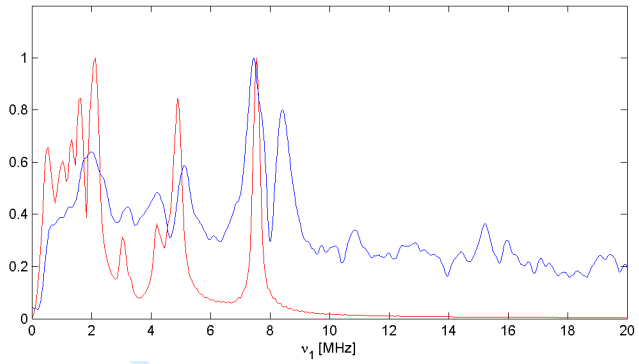

b) Spectral contributions of histidine nitrogens.

Green: simulated spectra; Blue: experiments.

The simulated spectra are the sum of the individual contributions of the two directly coordinating hisitidine nitrogens (simulation parameters given in Table 1 of the main text).

X-band HYSCORE spectra:

B_0=2268 G (g=g_z)

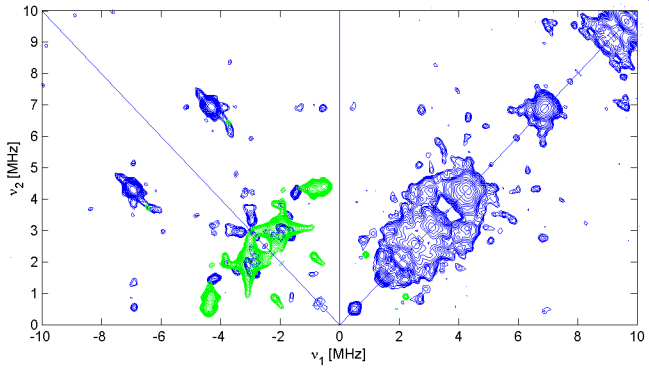

B_0=2500 G

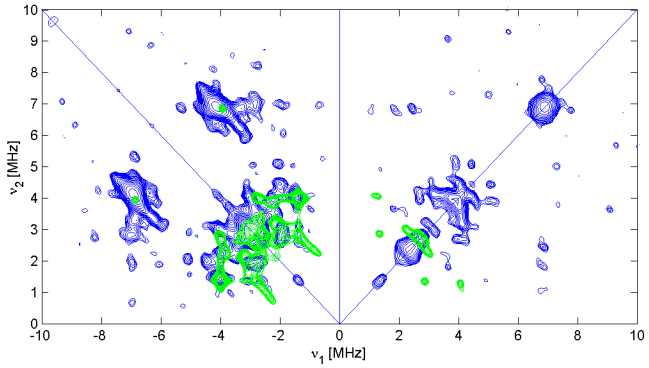

B_0=2900 G

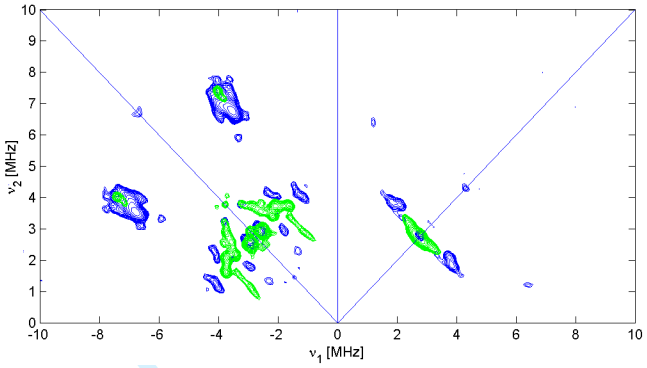

B_0=3123 G

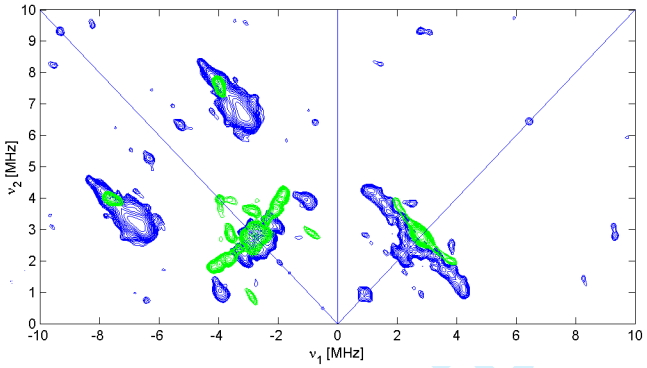

B_0=3374 G (g=g_y)

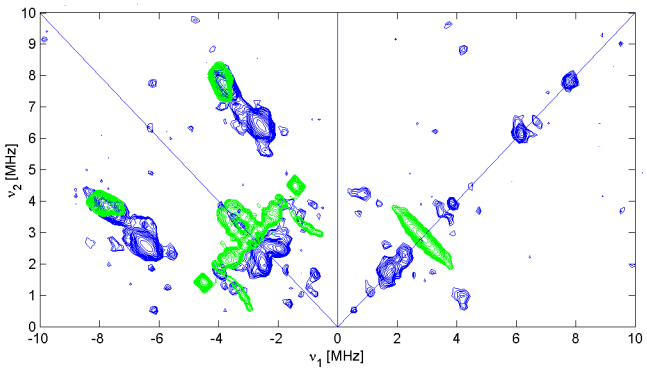

S-band HYSCORE

B_0=1750 G (g≈g_x)

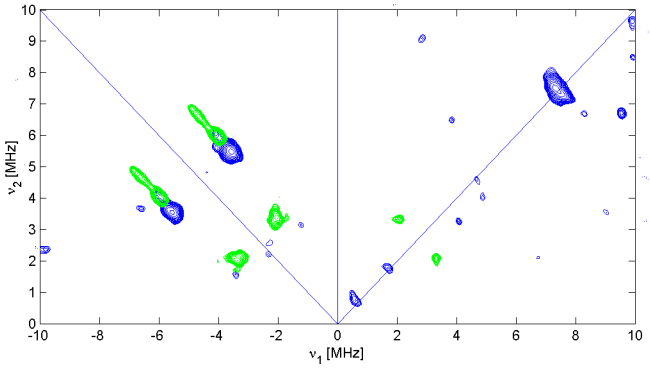

X-band 3-pulse ESEEM

B_0=5432 G (g=g_x)

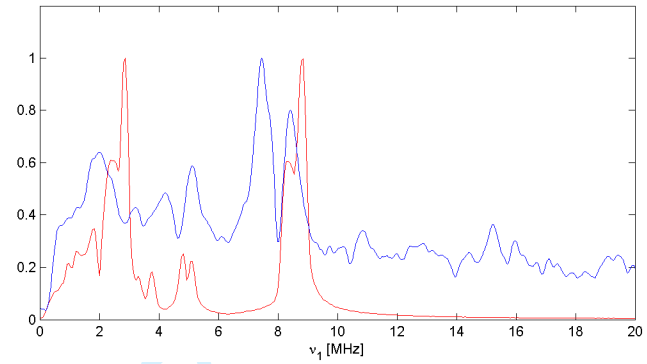

c) sum of histidine and heme contributions

X-band HYSCORE spectra

B_0=2500 G

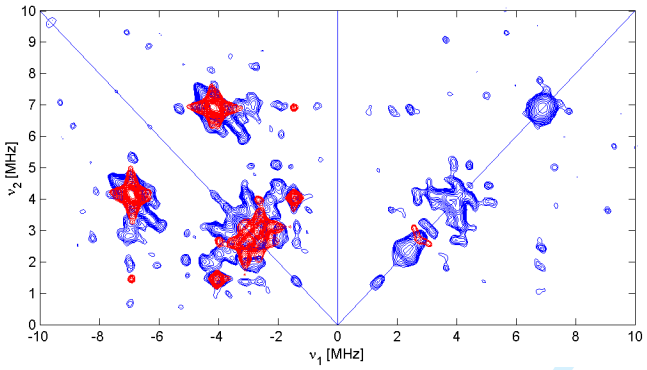

B_0=2900 G

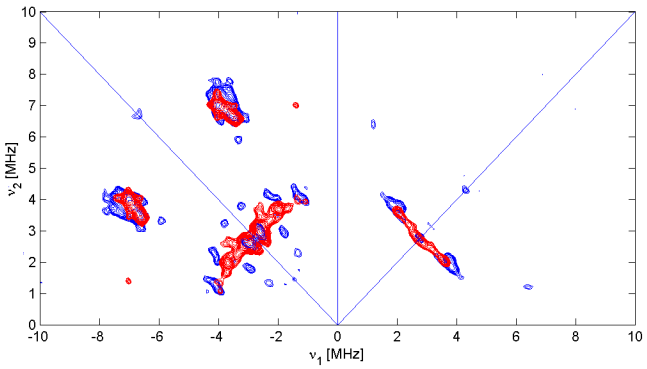

B_0=3123 G

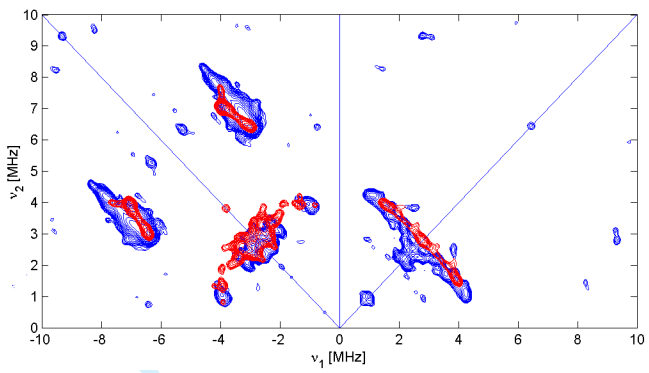

NOTE: all simulated spectra are the sum of the individual HYSCORE spectra for each nucleus (sum of two-spin (S=1/2, I=1) systems). Potential combination frequencies are hence not reproduced in the simulations. The relative intensity of the different peaks is also influenced by the summation. This is particularly apparent for the magnetic-field settings near $g=g_z$, where the DQ cross-peaks of the His nitrogens are not visible in the summed spectrum (see main text Figure 2c). However, the simulation using a three-spin system (S=1/2, I_{hemeN} = 1, I_{HisN}=1) reveals these DQ peaks:

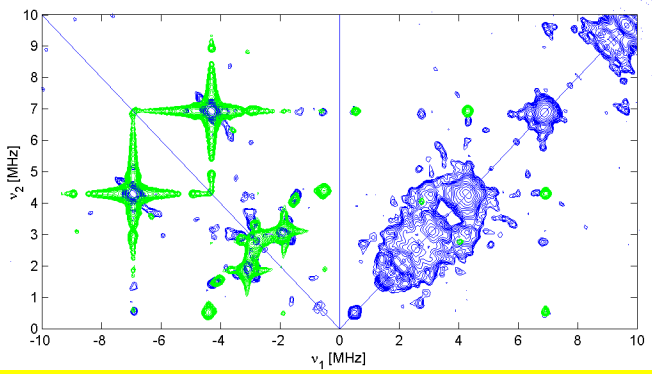

Similarly, part of the elongated DQ(heme) ridge found in the simulations shown in Figure 2d (main text) are partially suppressed in the experimental spectra by the strong DQ(His) cross-peaks (higher frequency part of ridge is weakly visible upon lowering of the contour lines in the experimental spectrum).

E7Q-CYGB

The absorption spectrum of the as reconstructed E7Q mutant of CYGB shows that the protein is partially in the ferric form and partially in the oxygenated ferrous form. The latter form is diamagnetic and does not contribute to the EPR spectrum.